Hydraulic deterioration of geosynthetic filter drainage system in tunnels – its impact on structural performance of tunnel linings

C. Yoo

Professor, School of Civil, Architectural Engineering and Landscape Architecture, Sungkyunkwan University, 2066 Seoboo-Ro, Jan-An Gu, Suwon, Kyong-Gi Do, Korea, E-mail: csyoo@skku.edu

Received 02 February 2016, revised 05 May 2016, accepted 05 May 2016

ABSTRACT: This paper presents the results of an investigation into the effect of decrease in drainage capacity by hydraulic deterioration of tunnel geosynthetic drainage systems on the structural performance of tunnel linings. The use of geosynthetics in tunnel construction is first introduced together with a summary of geotextile filter design principles and practices. A series of stress–pore-pressure-coupled finite-element (FE) analyses were then carried out on a number of tunnel cases in order to investigate the effect of hydraulic deterioration of the tunnel drainage layer on the structural performance of tunnel linings. It is shown that the decrease in drainage capacity of the drainage layer significantly increases the axial thrust and bending moment of the tunnel lining, with more pronounced increases in the bending moment. It is also revealed that hydraulic deterioration-induced lining forces tend to increase with the hydraulic head and slightly decrease with the cover depth. It is also shown that the progressive development of hydraulic deterioration-induced lining forces can be best fit with an exponential function which can be used to predict the lining force increase for a given tunnel condition. Practical implications of the findings are discussed.

KEYWORDS: Geosynthetics, Geotextile filter, Drainage, Tunnel, Lining, Clogging, Finite-element analysis, Stress–pore-pressure-coupled analysis

REFERENCE: Yoo, C. (2016). Hydraulic deterioration of geosynthetic filter drainage system in tunnels – its impact on structural performance of tunnel linings. *Geosynthetics International*. [http://dx.doi.org/10.1680/jgein.16.00010]

1. INTRODUCTION

Due to their cost-effectiveness, ease of installation, and well established mechanical and hydraulic properties, geosynthetics have become essential engineering materials in the field of geo-engineering (Koerner 2012). Geosynthetics are also heavily used in tunnel construction. For example, geotextiles and/or geocomposites are used as filter as well as drainage layers while geomembranes are used for watertightness. As a tunnel drainage system usually consists of geosynthetic filter layers and drain pipes, it is therefore of paramount importance to adopt the governing geotextile filter design principles when designing the drainage layer to optimise its performance during its service life.

There are vast case histories of damage in tunnel linings due to a decrease in drainage capacity of the tunnel drainage layer during operation (Lee *et al*. 1999; Shin *et al*. 2005, 2014). The decrease in drainage capacity of a tunnel drainage layer can be caused by the accumulation of transported material in its openings (clogging) and squeezing by ground loosening loads as well as concrete placement, which in turn results in the development of unwanted hydrostatic pressure build-up behind the tunnel lining (Shin *et al*. 2005). Such a mechanism is extremely important in drained tunnels constructed in soils as the chances of clogging the tunnel drainage system are higher for soft ground tunnels than for tunnels in rock (Lee *et al*. 1999; Park 1999; Celestino 2005; Franzen and Celestino 2002; Shin and Potts 2002; Shin 2008). Such a malfunction of a drainage layer eventually causes the long-term hydro-mechanical interaction between the ground and tunnel lining which governs the tunnel lining system behaviour. It is therefore of particular importance to understand the fundamental governing principles of geotextile filtration and to correctly evaluate the effect of a decrease in drainage capacity of a tunnel drainage system on the structural performance of the tunnel lining.

There are surprisingly few studies focusing on the hydro-mechanical interaction between lining and water-bearing ground that may arise due to the decrease in drainage capacity of a drainage layer in tunnels. Shin *et al.* (2005) performed pioneering work in this area, focusing on the hydro-mechanical interaction between the ground and the lining in New Austrian Tunnelling Method (NATM) tunnels in the event of deterioration of the tunnel drainage system. Bilfinger (2005) also investigated the lining load due to groundwater focusing on the comparison between impermeable and drained linings within the context of lining design. Later, Shin and his co-workers conducted a number of studies concerning the effect of local hydraulic deterioration caused by filter clogging on structural damage to the tunnel lining (Shin 2008; Jung *et al.* 2013; Shin *et al.* 2014). Although these studies highlighted insights into the hydro-mechanical interaction between the ground and the lining due to a change in hydraulic boundary conditions around the tunnel lining in the event of hydraulic deterioration, these studies are limited to idealised tunnel cases constructed in a fixed type of ground. No relevant studies have been directed at factors affecting the hydro-mechanical interaction between lining and ground in the event of decrease in drainage capacity of tunnel drainage layer under various boundary conditions.

In this study, the results of a numerical investigation into the effect of a decrease in drainage capacity of tunnel drainage layer, due to hydraulic deterioration, on the lining performance are presented specifically for drained tunnels. A number of hypothetical tunnel construction cases were first developed with due consideration of tunnel cover depth, as well as, depth of groundwater table, and ground type. The developed cases were then analysed using a stress–pore-pressure-coupled, finite-element model which can simulate the hydro-mechanial interaction that may arise due to hydraulic deterioration of a drainage layer. The results of the analyses are presented so that the structural performance of the lining and the hydro-mechanical ground-lining interaction in the event of hydraulic deterioration of drainage layer can be related. The following sections present the tunnelling and ground conditions, the two-dimensional finite-element modelling, and the practical implications of these findings.

2. TUNNEL DRAINAGE AND WATERPROING USING GEOSYTHETICS

A tunnel can be either sealed (waterproofed) or drained when constructed below the groundwater table, depending on how the groundwater ingress into the tunnel is handled. The tunnel behaviour and its environmental impact on surrounding areas are significantly affected by the way in which the groundwater is handled during the operation. In this section, the use of geosynthetics – geotextiles in particular – as drainage filters in drained tunnels is discussed within the frame work of conventional drill and blast tunnels.

2.1. Drained vs. undrained system

2.1.1. *Drained waterproofing system*

In a drained tunnel as shown in Figure 1a, a drainage system including drainage layers and pipes needs to be installed to prevent build-up of hydrostatic pressure on the final concrete lining. Flexible and continuous membranes are placed against the initial shotcrete lining prior to installation of the final concrete lining for waterproofing, backed by a geotextile or geocomposite as a drainage layer behind the geomembrane. Note, however, that a drained tunnel can also be sealed (waterproofed) in the sense that the water is guided to the longitudinal drainage pipes but is not allowed to enter the tunnel interior (Huang *et al.* 2009). To prevent unwanted hydrostatic pressure on the final lining, the drainage system must, therefore, be installed and maintained so as to be fully and permanently functional. Provided that the drainage system works as intended, no hydrostatic pressure acts on the final concrete lining, thus enabling thinner and more lightly reinforced liners to be designed. In a fractured rock mass, high groundwater inflows often enter drained systems (even after rock mass grouting) resulting in increased pumping costs. High inflows can also increase the deposition of calcium precipitate in pipes. For underwater tunnels such as subsea tunnels, full hydrostatic water pressure should be considered even with a drained system as the water table remains constant above the tunnels, unless an intensive grouting program is implemented in the surrounding ground.

Illustrated in Figure 1b are details of a typical drainage system. As shown, either fleece for low discharge or composite geosynthetics or air-gap membranes for high discharge is used in the interface between the shotcrete and concrete lining. The water discharge is secured using geosynthetics such as geospacers and geocomposite drains. Polyester should not be used as it can be destroyed by hydrolysis in an alkaline environment such as concrete (Kolymbas 2005). Although polyvinyl chloride (PVC) produces hydrochloric acid in case of fire, it may be used when covered by the concrete lining. The drainage layer receives the groundwater flowing to the crown and the sides of the tunnel and guides it to the longitudinal drainage pipes, which are installed where the sides merge with the invert. The interface drainage and the drainage pipes are embedded within granular filters (‘dry pack’), and the pipes are perforated in their upper parts.

2.1.2. *Undrained waterproofing system*

In undrained systems, a layer of geomembrane is installed around the entire tunnel envelope to prevent water seepage into the tunnel. When an undrained system is considered, the groundwater table will re-establish its original position after the installation of the final lining, thereby subjecting it to hydrostatic pressure. The tunnel invert geometry and the structural design of the lining must be adapted to accommodate for the hydrostatic head.

When constructed with high quality, the operations and maintenance costs are relatively low in comparison

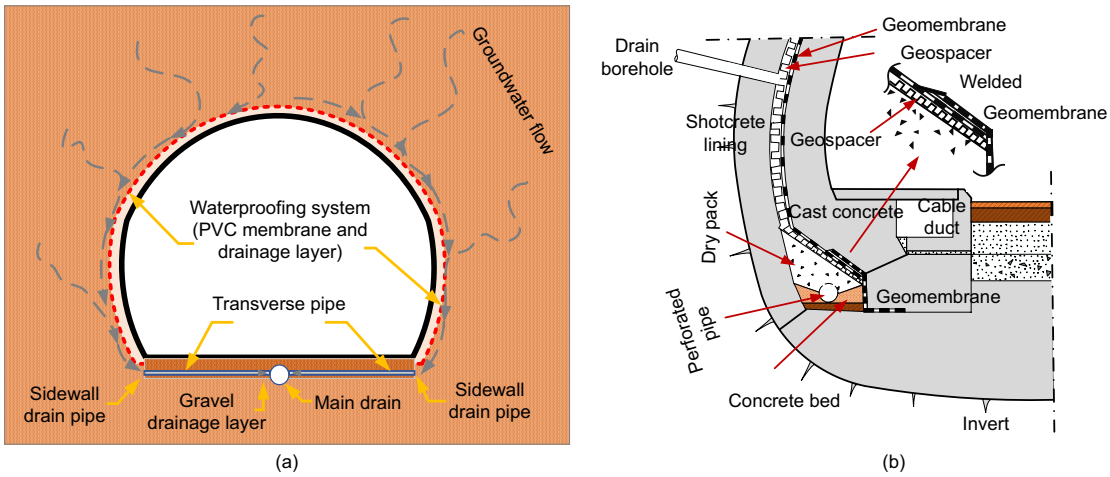

Figure 1. Schematic diagrams of drained tunnel and cross section of lining system: (a) drained tunnel; (b) cross-section of lining system (after Kolymbas 2005)

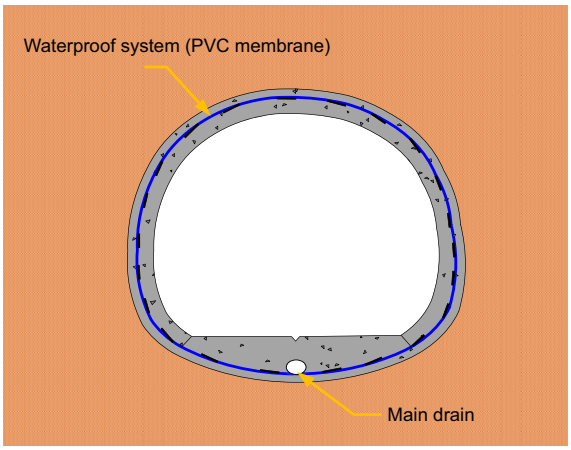

Figure 2. Schematic diagram of undrained waterproofed tunnel

with the drained system because of reduced pumping costs and much slower accumulation of calcite deposits. Figure 2 shows a typical undrained waterproofed tunnel. Table 1 gives comparison between drained and undrained systems.

3. CLOGGING OF DRAINAGE LAYER AND LINING LOAD

3.1. Geotextile filtration mechanism and design criteria

3.1.1. *Filtration mechanism*

To ensure the long-term performance of a drained tunnel, it is critical to have adequate filters which have the role of preventing soil and adjacent material particles from entering the drain while still allowing water to flow freely. When the filter does not retain the particles, the drain is at high risk of becoming clogged with transported sediments. On the other hand, when the filter openings themselves become obstructed, water is unable to reach the drain. It is therefore critical that geotextile filter layers used in tunnels are properly designed with due consideration of filter design principles.

Soil filtration by geotextiles involves complex interactions between the filter and contiguous soil (Lee and Bourdeau 2006). Five mechanisms have been identified such as piping, bridging, blinding, blocking (or plugging) and clogging (Rollin and Lombard 1988; Lafleur 1999). Of these five mechanisms, all but bridging, which can be considered a highly desirable condition, lead to a reduction in the drainage capacity by decreasing the permeability.

As indicated by Palmeira and Fannin (2002), a filter is a porous medium that acts primarily to retain the base soil against which it is placed without impeding the through-flow of groundwater seepage. As such, retention and permeability criteria govern filtration applications. In view of the tunnel drainage system, however, blocking and clogging are more relevant to the mechanisms that decrease permeability, which involve more local or internal action of the geotextile (Park 1999). In the case of blocking, coarse particles directly in contact with the geotextile surface obstruct the filter openings, preventing fine particles as well as fluid from penetrating. On the other hand, internal clogging is the direct result of penetration of migrating fine particles into the filter fabric causing fibre constrictions. Fines can then accumulate within the geotextile and obstruct its drainage channels. The time required for physical clogging to stabilise in a particular situation varies with the hydraulic gradient magnitude such that the greater the gradient, the faster the process. Internal clogging may also occur as a result of the precipitation of chemical substances or bacteriological activity in the geotextile pores. A schematic illustration of the blocking and clogging mechanism is given in Figure 3.

3.1.2. *Design criteria*

The geotextile filter design methodology essentially follows the same principles as those adopted for the graded granular filter. Filaments and fibres in a geotextile can be viewed as particles whereas pores are treated as voids but with a more complex geometric relationship than a soil. The design criteria for geotextile filters consist of; (1) a retention criterion to ensure the geotextile openings are small enough to prevent excessive migration

Table 1. Comparison of drained and undrained tunnels

	Drained tunnel	Undrained tunnel
Construction	• Geosynthetics such as geotextiles, geospacers, and geocomposite drains are placed in the interface between shotcrete and concrete lining to provide a stable interface for water discharge	• Geomembranes are placed in the shotcrete and concrete lining interface for a complete waterproofing.
Advantages	• Can reduce hydrostatic pressure acting on final lining → reduction in lining thickness	• Easy maintenance • Low construction cost • Low environmental impact associated with groundwater
Disadvantages	• Maintenance cost can be high • Environmental impacts associated with groundwater lowering may occur • High construction cost	• Requires thicker final lining due to higher hydraulic head • Repair for leakage requires considerable work and the associated cost is high

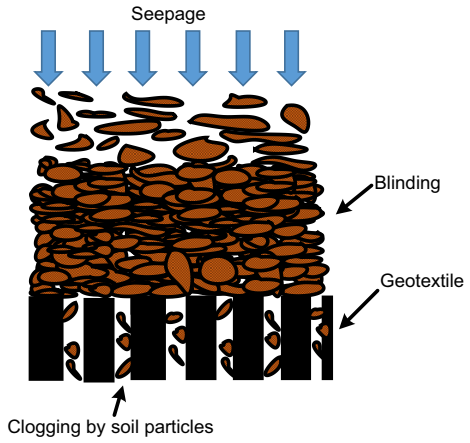

Figure 3. Illustration of blinding and clogging

of soil particles which is known as 'piping'; (2) a permeability criterion to ensure the geotextile is permeable enough to allow liquid to pass through relatively unhindered so that excess pore pressure does not build up behind it; and (3) an anti-clogging criterion to ensure the ability of the geotextile to maintain its permeability when soil particles are entrapped in the geotextile. Note here that the survivability and durability criteria should also be considered for long-term performance.

Selection of a candidate geotextile for routine filtration applications is often made with reference to available design criteria based on empiricism. For critical or severe applications, or when warranted, performance testing is required such as a permeameter test described in the ASTM *Test Method for Measuring the Filtration Compatibility of Soil-Geotextile Systems* (D5101-12) (ASTM).. Details of the design criteria and the filtration performance test are beyond the scope of this paper but available elsewhere (Lee and Bourdeau 2006).

There have been a few studies on the applicability of the available filter design criteria to geotextile filters used in tunnels including Park (1999) and Moon (2000). In particular Moon (2000) selected two tunnel sites in Seoul, Korea in order to check the validity of the filter design practice. In his study, the compatibility of soils surrounding tunnels and two types of candidate geotextiles (nonwoven needle-punched) was checked by performing a series of gradient ratio (GR) tests with different hydraulic gradients (i) of up to $i = 5$. Tables 2 and 3 summarise the properties of the soils and the geotextiles used in the tests. The test results were then compared with the empirical design criteria as listed in Table 4. The results indicated that the retention and permeability requirements were in accordance with those from the performance tests. As shown in Table 4, the candidate geotextile filters however failed to satisfy the majority of the clogging criteria even though the GR tests yielded GR values not exceeding 3. These results suggest some degree of inherited conservatism in the clogging resistance criteria as other researchers have indicated (Christopher and Fischer 1992; Palmeira and Fannin 2002). Details of the test results are available elsewhere (Moon 2000). Further in-depth studies in this area are warranted.

3.2. Hydro-mechanical interaction of groundwater and lining

Interaction between the water pressure and the tunnel lining for a drained tunnel depends greatly on the performance of the drainage layer. As illustrated in Figure 4a, little or no water pressure acts on the final lining when the drainage layer works as intended. When the drainage capacity of the drainage layer decreases, on the other hand, the water pressure acts directly on the final lining, leading to increases in lining forces (Figure 4b). In such cases the degree of lining force increase is influenced by a number of factors, such as the relative ground-lining stiffness, the relative ground-lining permeabilities, and geometric factors (Bilfinger 2005; Yoo 2005; Shin 2008; Murillo *et al.* 2014). Unwanted water pressure due to a decrease in drainage capacity, not considered in design, can impose additional lining forces, which could induce structural damage to the lining when excessive as shown in Figure 5.

4. PARAMETRIC STUDY

A series of stress–pore-pressure-coupled, finite-element (FE) analyses were conducted in order to gain insight into the effect of a decrease in drainage capacity of the drainage layer by hydraulic deterioration on the structural performance of tunnel lining. Details of the parametric

Table 2. Grain size characteristics of soils (after Moon 2000)

Properties	Soil A	Soil B
Natural water content, w(%)	16.7	24.8
Specific gravity, G_s	2.60	2.68
Void ratio, e	0.41	0.50
Maximum dry unit weight, γ (kN/m^3)	18.5	17.8
Optimum water content, w_{opt} (%)	11.5	14.5
Coefficient of uniformity C_u	25.4	12.0
Coefficient of curvature, C_c	2.37	1.02
D_{15} (mm)	0.12	0.04
D_{50} (mm)	1.1	0.14
D_{85} (mm)	4.1	3.0
D_{90} (mm)	4.4	4.7
Unified Soil Classification System	SW-SM	SM
Permeability, k_s (m/s)	8.1×10^{-6}	1.6×10^{-6}

Table 3. Opening size and permeability properties of candidate geotextiles (after Moon 2000)

Properties	Geotextile A	Geotextile B
Dry sieving O_{95} (mm)	0.12	0.09
Hydrodynamic sieving O_{95} (mm)	0.08	0.06
Permeability, k_d (m/s)	3.8×10^{-3}	2.7×10^{-3}

study and the results are presented under the subsequent subheadings.

4.1. Tunnel cases considered

In this study, a number of tunnel construction scenarios were considered in which a 7 m diameter circular drained tunnel is constructed under various boundary conditions. In order to cover a wide range of tunnel cases, the tunnel cover depth (H_c) and the hydraulic head above the tunnel crown (H_w) were varied as $H_c = 3D$, $5D$, $10D$ and $H_w = 1D$, $2.5D$, $3D$, $4D$, $5D$ where D is the tunnel diameter. Three ground types were considered ranging from decomposed granitic soil (GT-I) to poor (GT-II) and fair (GT-III) rocks, as per the engineering classification of rocks (Waltham 1994). Figure 6 shows a schematic diagram of the tunnelling conditions considered in this study.

For simplicity, a 0.3-m thick unreinforced concrete lining was assumed as a final lining for all tunnels although thicker steel-reinforced concrete linings may be adopted in some of the tunnels constructed in weak ground (i.e. GT-I) considered in this study. A typical drainage system was assumed to be installed behind the lining. Table 5 summarises the geotechnical properties of the various ground types as well as the mechanical properties of the lining considered in this study. Note that these values were taken from a design case history (Yoo and Kim 2008; Yoo *et al*. 2012).

4.2. Stress–pore-pressure-coupled, finite-element analysis

A commercial FE software package Abaqus (2011) was used for analysis. The stress–pore-pressure-coupled effective stress formulation available in Abaqus (2011) was adopted in order to realistically capture the hydro-mechanical interaction mechanism between the lining and the groundwater in the event of hydraulic deterioration of the drainage layer. Fundamentals of the stress–pore-pressure-coupled formulation can be found in the Abaqus user's manual (Abaqus 2011).

4.2.1. *Finite-element modelling*

A two-dimensional FE modelling approach was adopted for this study. Figure 7 shows the two-dimensional, FE model adopted for cases with a cover depth of $H_c = 5D$. As shown, the FE model extends to a depth of $4D$ below the tunnel invert, while the lateral boundaries extend to a distance of $10D$ from the tunnel centre. At the vertical boundaries, displacements perpendicular to the boundaries were restrained whereas pin supports were placed at the bottom boundary. The locations of the boundaries were selected based on a preliminary analysis so that boundary effects on the stress–strain–pore pressure solution can be minimised. In a stress–pore-pressure-coupled analysis, hydraulic boundary conditions are also required in addition to the displacement boundary conditions. With reference to Figure 7, a no-flow condition was assigned to the bottom boundary and the groundwater level was assumed to remain constant at its original level throughout the analysis.

The region above the groundwater table was discretised using plane strain eight-node displacement elements with reduced integration (CPE8R) while displacement and pore pressure elements (CPE8RP) were used for the region below the groundwater table. The three node beam element (B22) was used for the concrete lining. A layer of continuum elements was designated as a dummy lining to which the mechanical properties of the ground were assigned but with the permeability for concrete, i.e. $k_c = 1 \times 10^{-10}$ m/s. This modelling scheme, originally proposed by Shin and Potts (2002), was necessary as the beam element representing the concrete lining cannot handle hydro-mechanical interactions. The geotextile filter/drainage layer was modelled using a thin layer of continuum elements (CPE8R) behind the concrete lining.

Table 4. Results of clogging resistance evaluation (after Moon 2000)

Method	Criterion	Geotextile A		Geotextile B		Remarks
		Soil A	Soil B	Soil B	Soil A	
Christopher and Holtz (1985)	$O_{95}/D_{15} \geq 3$	0.5	1.5	1.0	0.33	Clogging
French Committee on Geotextiles and Geomembranes (1986)	$O_f/D_{15} \geq 4$	0.67	2.0	1.5	0.5	Clogging
Fischer *et al.* (1990)	$O_{50}/D_{50} \geq 0.2$	0.018	0.14	0.09	0.012	Clogging
Koerner (1990)	Percent open area $\geq 40\%$	92%	92%	91%	91%	No clogging

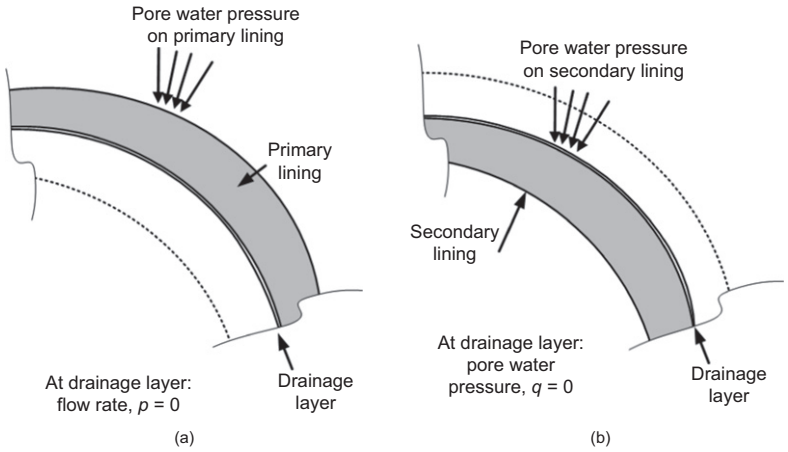

Figure 4. Water pressure – tunnel lining interaction in double-shelled tunnel (after Shin *et al.*, 2002): (a) no clogging; (b) clogging

Figure 5. Photo of damaged tunnel lining due to water pressure: (a) photo 1; (b) photo 2

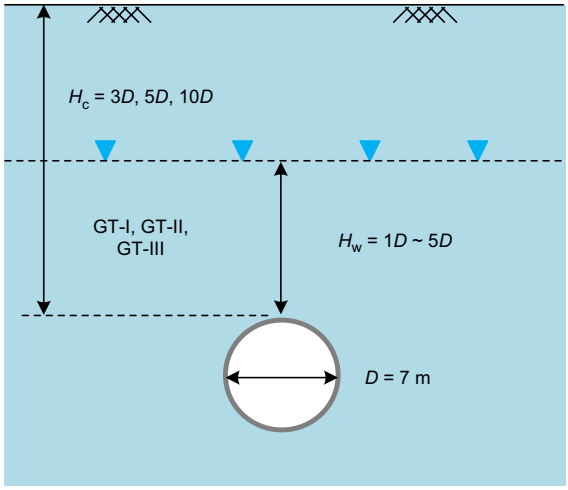

Figure 6. A schematic diagram of tunnel cross section

With regard to the material constitutive modelling, the ground was assumed to be an elasto-plastic material conforming to the Mohr–Coulomb failure criterion together with the non-associated flow rule proposed by Davis (1968), while the concrete lining was assumed to behave in a linear elastic manner. Note that a dilatancy angle of $\varphi = 20°$ was assumed for all ground types.

4.2.2. *Simulation strategy*

Figure 8 illustrates the modelling strategy adopted in this study. As shown, initial stress and pore pressure conditions were first established assuming the pore pressure below the groundwater level was hydrostatic. The tunnel excavation and lining installation were then executed for 10 days by adding and removing corresponding elements. For the excavation boundary, a zero pore pressure flow boundary condition was assigned to allow for water inflow to occur into the tunnel. The operation phase was then simulated in the subsequent step for 10 years during which the hydraulic deterioration of the drainage system was simulated.

During the initial and excavation stages, i.e. Steps I and II, the drainage layer was assumed to have the mechanical and hydraulic properties of the surrounding ground. In Step III, i.e. the operational stage, the permeability of the drainage layer (k_d) was then changed depending on the hydraulic deterioration level while keeping the mechanical properties unchanged.

5. RESULTS AND DISCUSSION

The results of the parametric study are presented in terms of the hydraulic deterioration-induced lining forces and stresses so that the effect of hydraulic deterioration of the drainage layer on the structural performance of the lining can be identified.

5.1. General characteristics

Illustrated in Figure 9 are the effect of decrease in permeability of the drainage layer on the change in lining forces (ΔSF, ΔSM) as well as stresses ($\Delta\sigma$) during operation for

Table 5. Material properties of ground and concrete lining

Parameter	GT-I	GT-II	GT-III	Lining
Saturated unit weight, γ_{sat} (kN/m^3)	25	25	25	25
Cohesion, c' (kPa)	5	100	500	–
Internal friction angle, ϕ' (deg)	30	35	35	–
Young's modulus, E (MPa)	16	100	500	2.3×10^3
Poisson's ratio, v	0.20	0.2	0.2	0.2
Lateral stress coefficient, K_o	0.5	0.5	0.5	–
Permeability, k_g (m/s)	4.4×10^{-5}	4.4×10^{-7}	4.4×10^{-8}	–

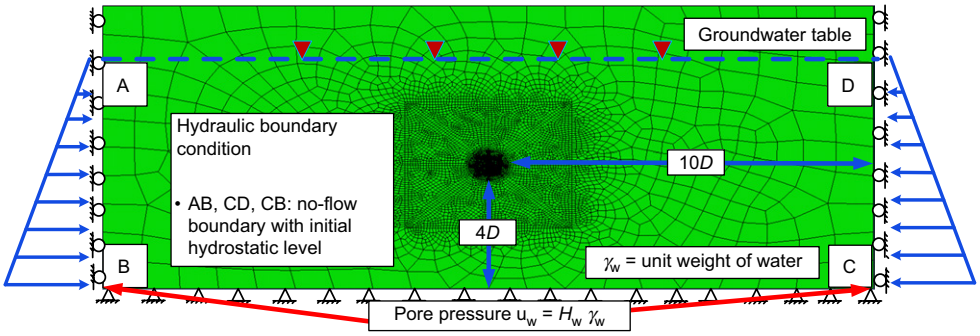

Figure 7. Two dimensional finite-element model adopted

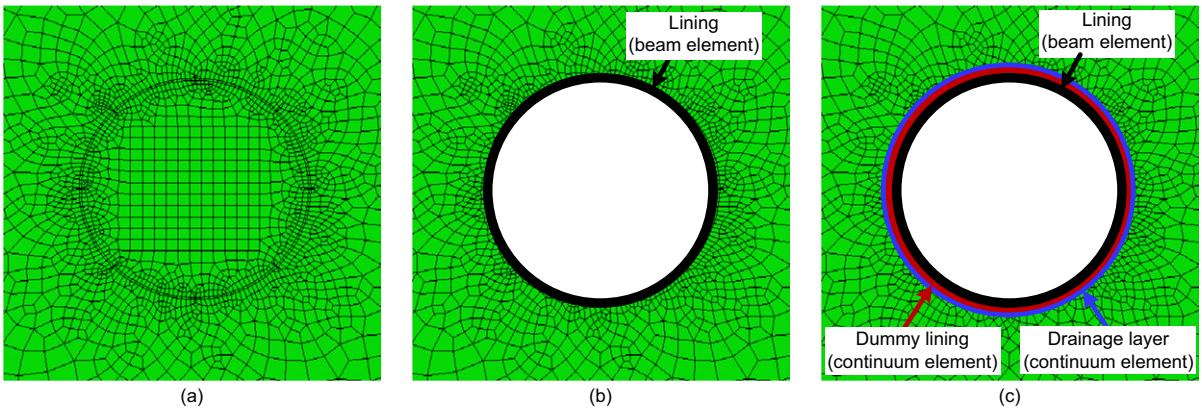

Figure 8. Modelling scheme adopted: (a) Step I: initial condition; (b) Step II: excavation and lining installation; (c) Step III: operation (hydraulic deterioration)

the baseline condition (GT-II, $H_c = 5D$, $H_w = 5D$). Note here that a range of permeability values of the drainage layer was considered by varying the relative permeability of the ground to that of the drainage layer, defined as $RP = k_g/k_d$, in the range of $RP = 1 \sim 1000$. In fact, the relative permeability represents the degree of hydraulic deterioration, such that the greater the RP, the higher the hydraulic deterioration level.

As shown in Figure 9, the development of additional lining forces, thus stresses, becomes evident as RP increases, illustrating that the decrease in the permeability of drainage layer in fact imposes additional lining forces. More specifically, the cases with $RP = 0.1 \sim 30$ show almost no additional lining forces and therefore can be considered as those with a fully functional drainage layer. When RP = 1000, which can be considered a fully deteriorated case, the hydraulic deterioration tends to increase axial thrusts in tension at the crown and the invert by as much as 0.05 MN while at the spring line of 0.08 MN in compression. Additional bending moments as high as 22 kN-m are also developed at the spring line while similar magnitudes of bending moments but in the opposite direction are developed at the crown and invert. The hydraulic deterioration-induced lining forces, in fact, result in increases in the lining stress in tension at the crown and invert levels, i.e. $315° \leq \theta \leq 45°$ and $135° \leq \theta \leq 225°$ (θ is measured clockwise from the crown), but in compression at the spring line, i.e. $\pm 45° \leq \theta \leq \pm 135°$ as shown in Figure 9c. When RP = 1000, the hydraulic deterioration leads to increases in the lining stresses $\Delta\sigma$ as great as 2 MPa, which corresponds approximately to a 10% increase from the no hydraulic deterioration case.

The variation of hydraulic deterioration-induced lining forces at the spring line with the relative permeability of the drainage layer is shown in Figure 10. Note here that the hydraulic deterioration-induced lining forces, ΔSF and

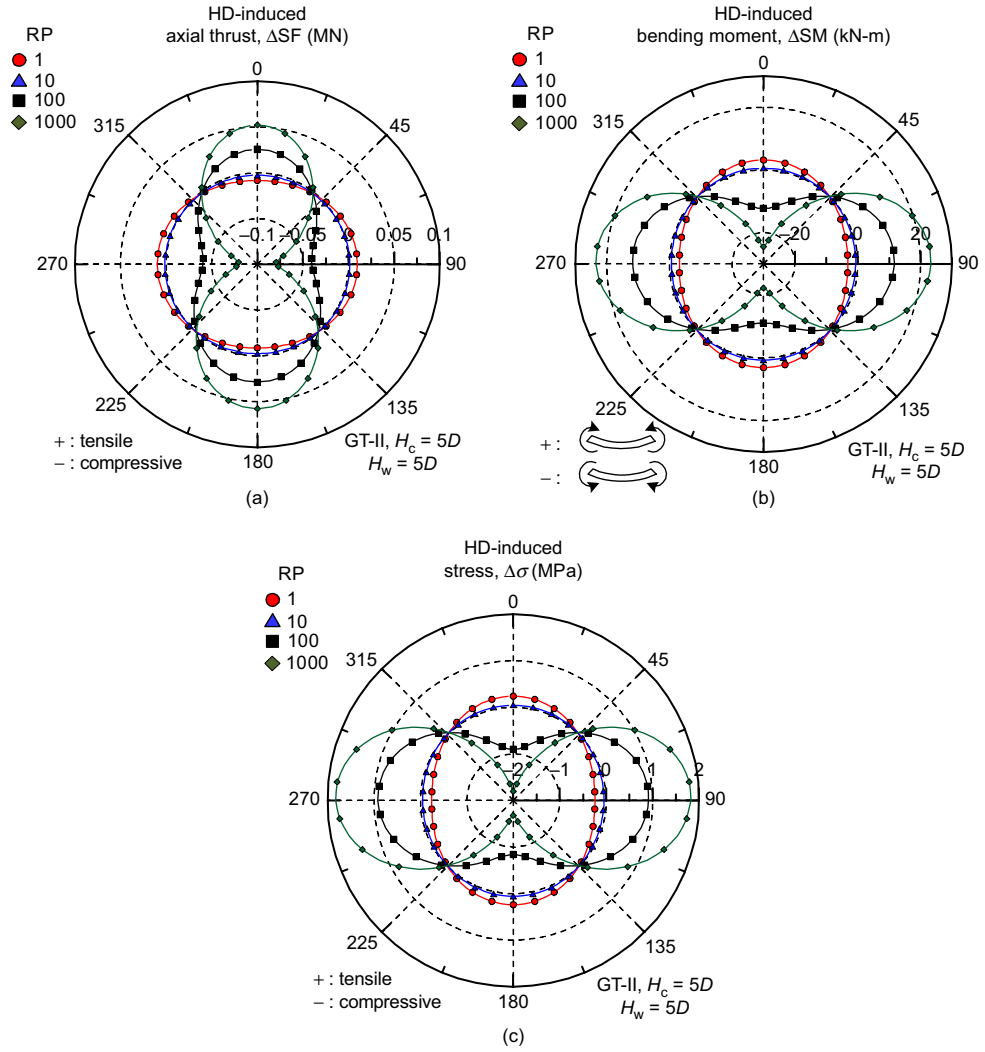

Figure 9. Hydraulic deterioration-induced lining force and stress distributions for various relative permeabilities (GT-II, $H_c = 5D$, $H_w = 5D$: (a) ΔSF; (b) ΔSM; (c) Δσ. HD, hydraulic deterioration

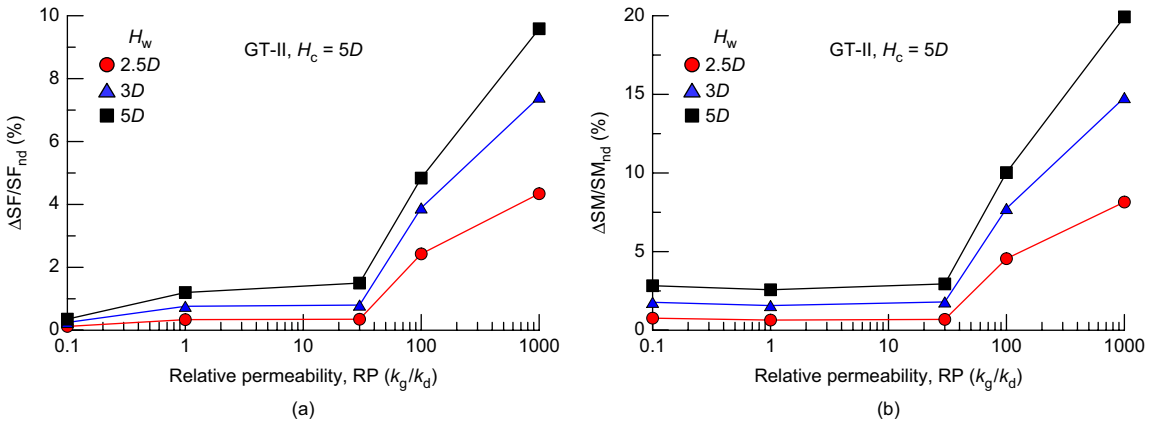

Figure 10. Variation of hydraulic deterioration-induced lining forces at spring line with *RP* (GT-II, $H_c = 5D$): (a) ΔSF/SF$_{nd}$; (b) ΔSM/SM$_{nd}$

ΔSM, are expressed in terms of percentage increase from the no hydraulic deterioration case as ΔSF/SF$_{nc}$ and ΔSM/SM$_{nc}$. As shown, an increasing trend of ΔSF/SF$_{nc}$ and ΔSM/SM$_{nc}$ with an increase in RP can be observed for a given hydraulic head H_w with a more pronounced increase when H_w is higher, suggesting that the decrease in drainage capacity of the drainage layer by hydraulic deterioration can impose more serious structural damage to the lining when the hydraulic head is high. The percentage increase for a given RP is larger for the bending

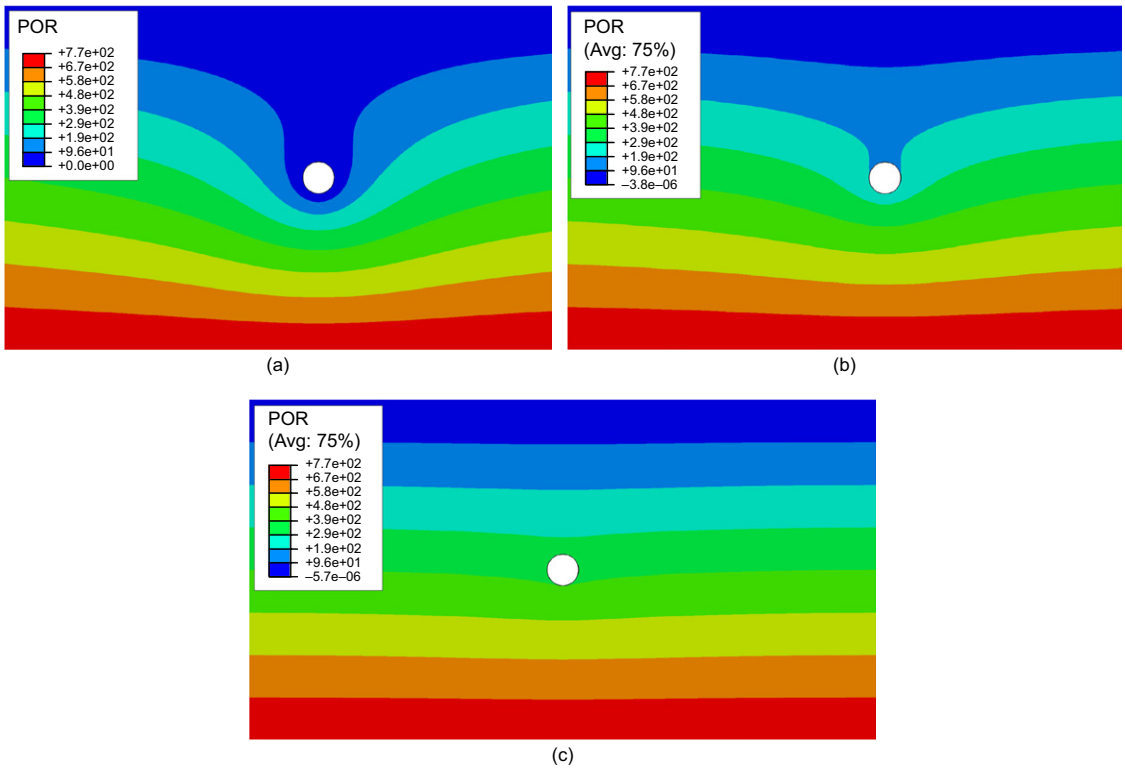

Figure 11. Pore pressure distributions (GT-II, $H_c = 5D$, $H_w = 5D$, unit = kPa): (a) RP = 1; (b) RP = 100; (c) RP = 1000

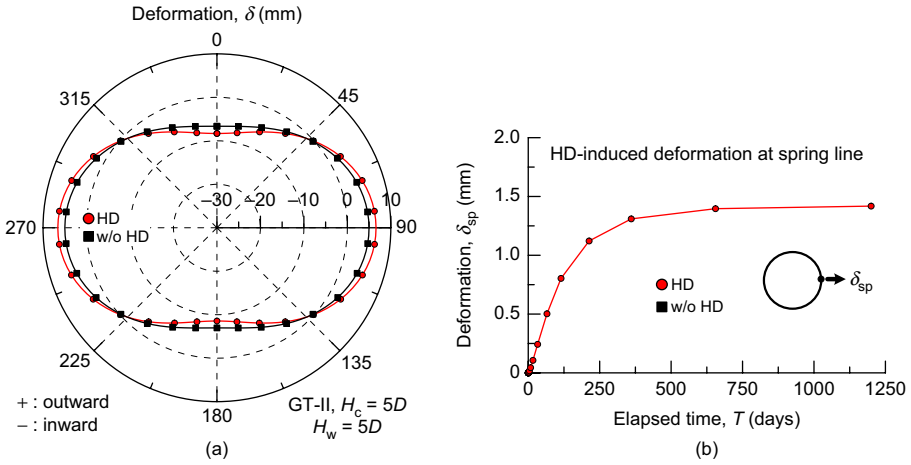

Figure 12. Hydraulic deterioration-induced lining deformation (GT-II, $H_c = 5D$, $H_w = 5D$, RP = 1000): (a) deformed profile; (b) progressive development of δ_{sp}. HD, hydraulic deterioration

moment than for the axial thrust showing a maximum increase of 10 and 20%, respectively, for $\Delta SF/SF_{nc}$ and $\Delta SM/SM_{nc}$ as shown in Figure 10.

The tendency of the lining force to increase due to hydraulic deterioration of the drainage layer is closely associated with pore pressure development around the tunnel lining caused by the permeability reduction in the drainage layer as illustrated in Figure 11 for the baseline case. As shown in these figures, for the case with a fully functioning drainage system, i.e. RP = 1, pore pressures around the lining appear almost zero. The pore pressure build-up around the lining becomes evident as RP increases with full hydrostatic pore pressures being developed when RP = 1000, i.e. a fully deteriorated case.

The pore pressure increase behind the lining in fact induces additional lining deformation as shown in Figure 12, in which the hydraulic deterioration-induced tunnel lining deformation in terms of the deformed profile and the progressive development with time are shown for the baseline case. As shown, the hydraulic deterioration induces additional lining distortion with a maximum deformation as high as 1.4 mm at the spring line. Time dependency of the hydraulic deterioration-induced lining deformation is well illustrated in Figure 12b, in which the hydraulic deterioration-induced lining deformation gradually increases with time until approximately 400 days after the start of hydraulic deterioration, after which it converges to its asymptotic value of 1.4 mm.

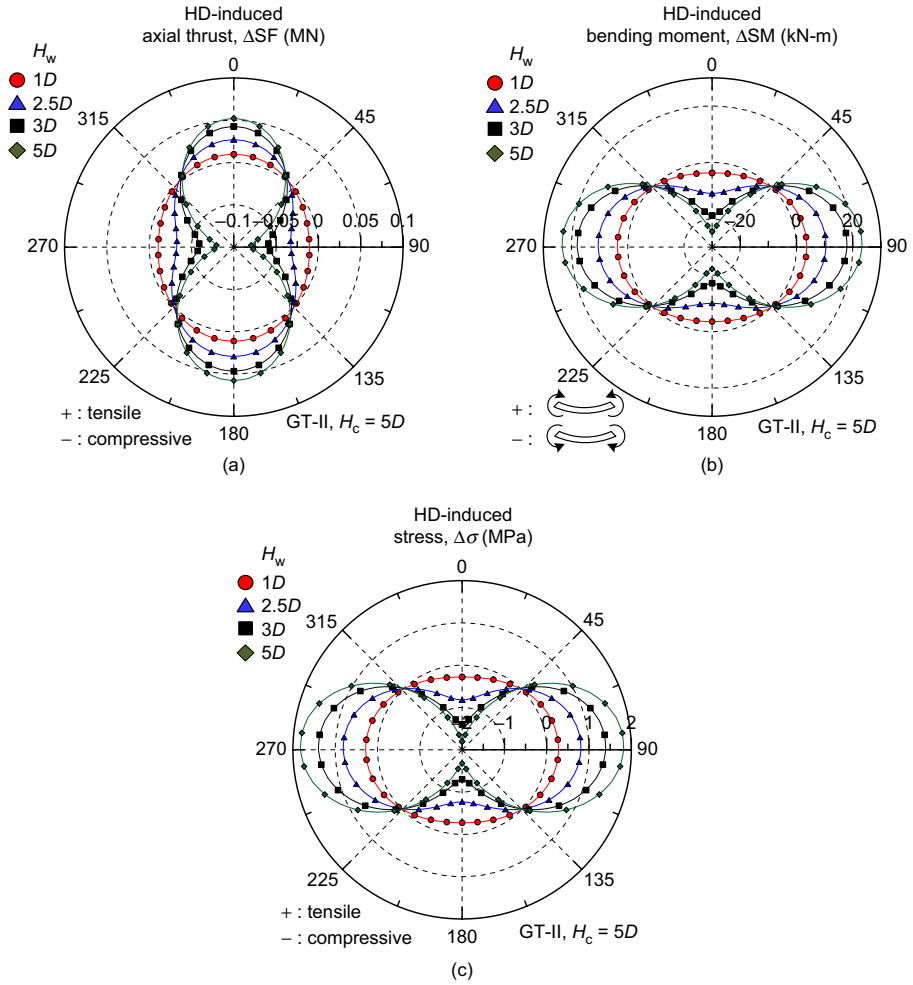

Figure 13. Hydraulic deterioration-induced lining force and stress distributions for various H_w (GT-II, $H_c = 5D$, RP = 1000): (a) ΔSF; (b) ΔSM; (c) $\Delta\sigma$. HD, hydraulic deterioration

5.2. Effect of hydraulic head

As indicated, it is known that the degree of reduction in permeability of a drainage system depends largely on the hydraulic gradient for a given loosening load (Lee *et al.* 1999). In a general sense, it can be stated that the larger the hydraulic head (H_w), the greater the hydraulic gradient. The effect of hydraulic head H_w on the hydraulic deterioration-induced lining forces are examined in relation to the tunnel cover depth H_c. The results presented here are relevant for fully deteriorated tunnel cases, i.e. RP = 1000, constructed in the ground type GT-II, unless otherwise indicated.

In Figure 13, the hydraulic deterioration-induced lining force distributions are shown for the hydraulic heads considered with a fixed cover depth of $H_c = 5D$. As noticed, a clear trend of increasing lining forces (ΔSF and ΔSM) with an increase in H_w is evident with the largest increase at the spring line. These hydraulic deterioration-induced lining forces impose additional stresses to lining as high as $\Delta\sigma = 1.8$ MPa, as shown in Figure 13c. Depending on the existing stress state, such stress increases can be a threat to the structural integrity of the lining.

The results in Figure 13 were rearranged in Figure 14 in which the hydraulic deterioration-induced lining forces and stresses at various locations are presented for various H_w. As seen, ΔSF and ΔSM increase linearly to 0.08 MN and 25 kN-m, respectively, for an increase of H_w from 1D to 5D. The percentage increase in the values of ΔSF and ΔSM from the otherwise fully drained case shown in Figure 15 indicate that the percentage increases of ΔSF of (0.5 ~ 3)% are much smaller than those of ΔSM (2 ~ 20)%, suggesting that the pore pressure build-up behind the lining is relevant to the increases in bending moment. In terms of the lining stress, the percentage increases for the range of H_w seem to follow the same trend observed in ΔSF and ΔSM, showing a maximum percentage increase of approximately 10% from the fully drained case when $H_w = 35$ m.

The progressive development of ΔSF and ΔSM at the spring line during operation for the various values of H_w considered are illustrated in Figure 16. Salient features that can be observed in these figures are two-fold. First, as shown in Figures 16a and 16b, the hydraulic deterioration-induced axial thrust ΔSF and bending moment ΔSM tend to gradually increase with time until converging to their maximum values, the general trend of which essentially follows an exponential function. These data are further normalised by their respective maximum values as presented in Figure 16c. As can be seen in this figure, the data tend to follow a trend line, irrespective of the locations, namely crown, invert and spring line, as well as the water depth H_w. The two-term exponential function

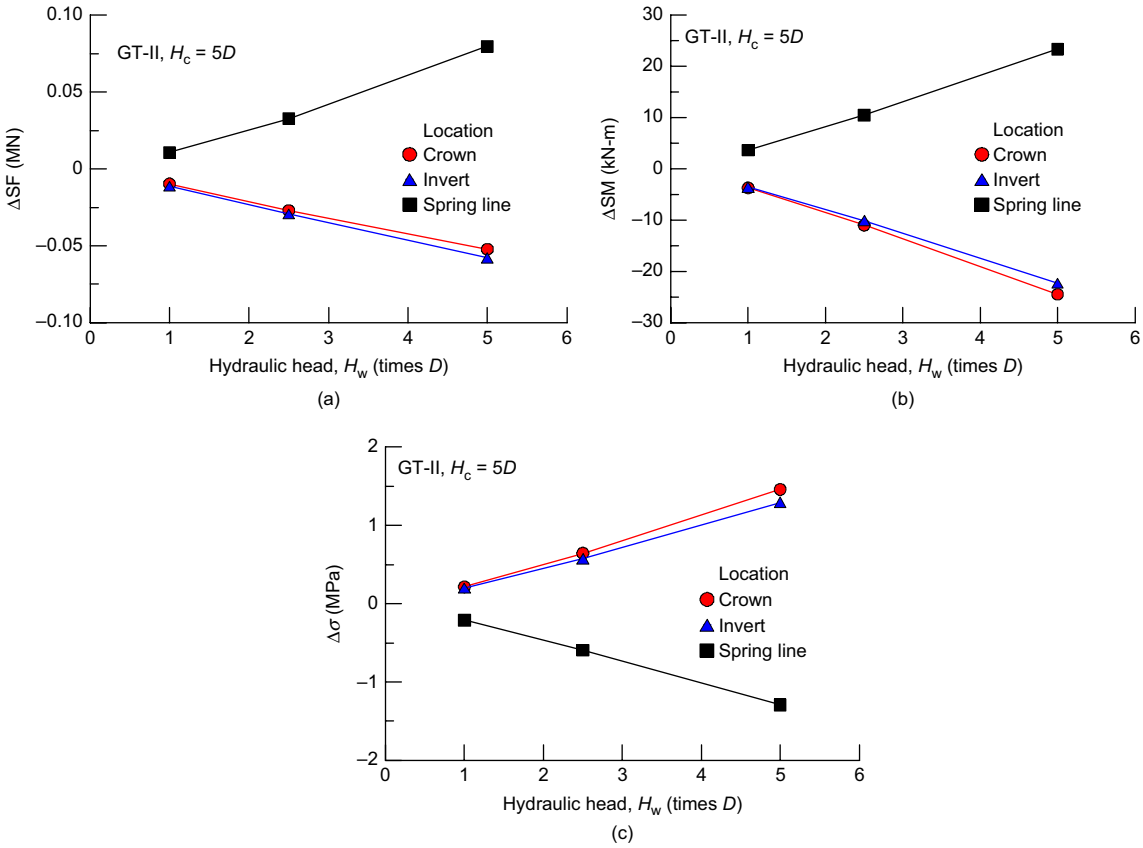

Figure 14. Variation of hydraulic deterioration-induced lining forces and stresses with H_w at various locations (GT-II, $H_c = 5D$, RP = 1000): (a) ΔSF; (b) ΔSM; (c) $\Delta\sigma$

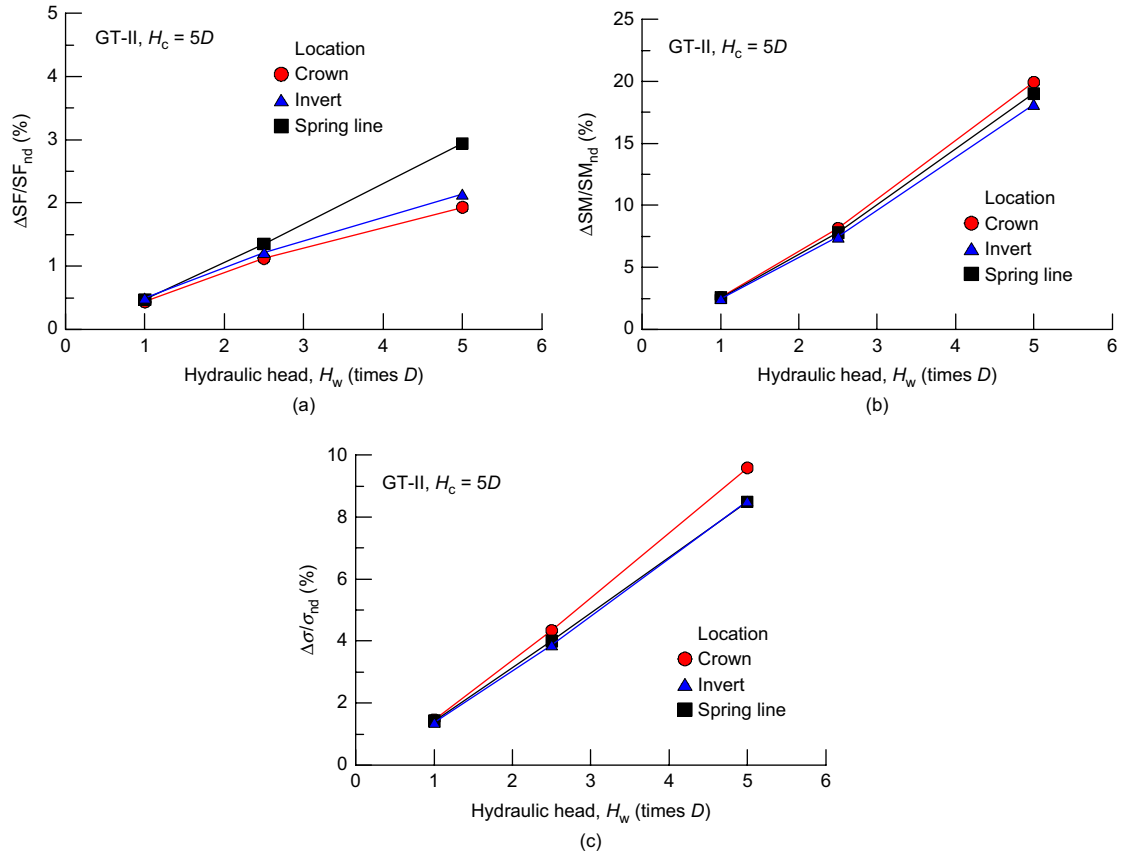

Figure 15. Variation of percent increase in hydraulic deterioration-induced lining forces and stresses with H_w at various locations (GT-II, $H_c = 5D$, RP = 1000): (a) $\Delta SF/SF_{nd}$; (b) $\Delta SM/SM_{nd}$; (c) $\Delta\sigma/\sigma_{nd}$

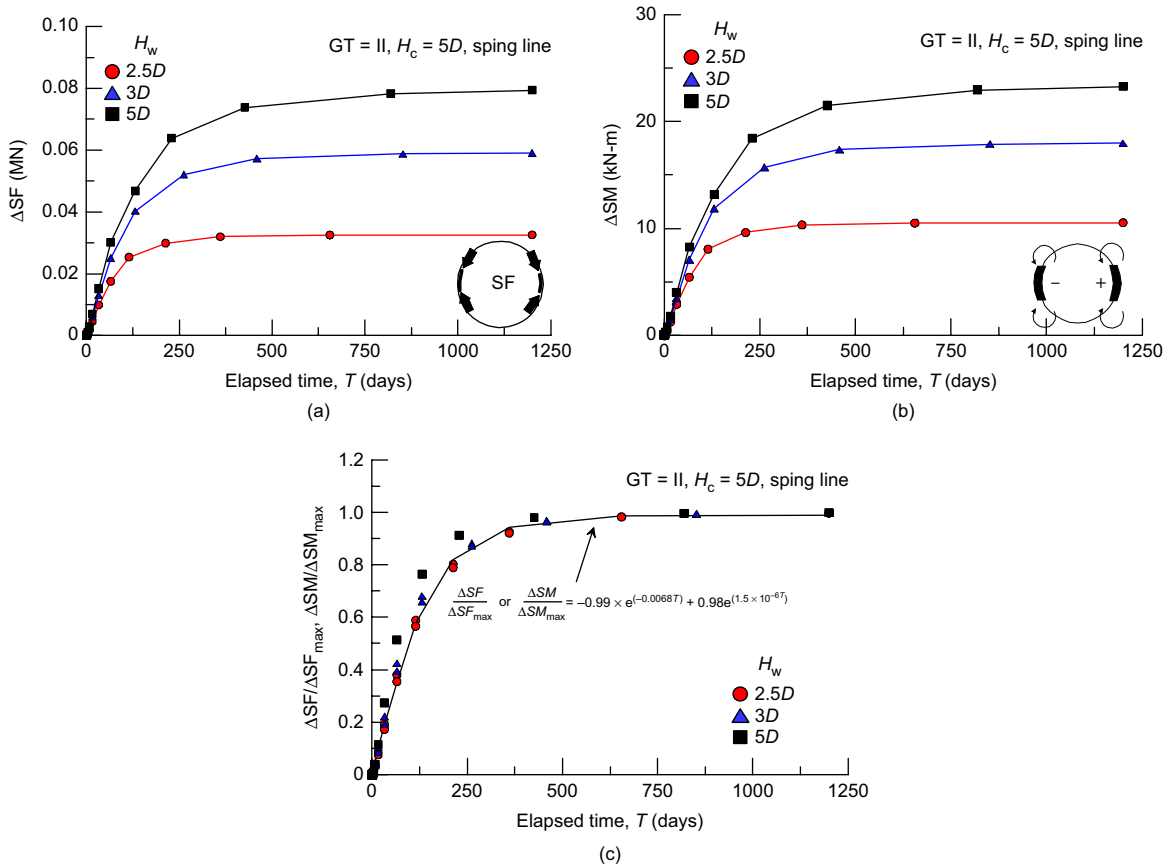

Figure 16. Progressive development of hydraulic deterioration-induced lining forces (GT-II, $H_c = 5D$, RP = 1000): (a) ΔSF; (b) ΔSM; (c) $\Delta SF/SF_{max}$ and $\Delta SM/SM_{max}$

defined by Equation 1 in essence provides an excellent fit to these data with $R^2 > 0.95$. Equation 1 can therefore be used to infer hydraulic deterioration-induced lining forces during operation for the range of cases considered in this study, given the respective maximum values.

$$\frac{\Delta SF}{\Delta SF_{max}} \text{ or } \frac{\Delta SM}{\Delta SM_{max}} = -0.99 \times e^{(-0.0068T)} + 0.98e^{(1.5\times10^{-6}T)} \quad (1)$$

where T is time in days after lining installation.

5.3. Effect of cover depth

Figures 17–19 show the results concerning the effect of cover depth H_c on the hydraulic deterioration-induced lining forces and stresses for the cover depths considered, i.e. $H_c = 3D$, $5D$, $10D$ while keeping $H_w = 5D$. As shown in Figure 17, it seems that the hydraulic deterioration-induced lining forces as well as stresses tend to slightly decrease with an increase in the cover depth H_c. Such an observation can also be noticed in Figure 18 and Figure 19 in which the hydraulic deterioration-induced lining forces/stresses and their normalised values are shown. In Figure 18, although not significant, it can be seen that ΔSM at the spring line decreases from 15 to 9 kN-m for an increase in H_c from $3D$ to $10D$. A similar trend can also be observed in Figure 19 where $\Delta SM/SM_{nc}$ decreases from 20 to 12% for an increase in H_c from $3D$ to $10D$, suggesting that the effect of hydraulic deterioration of the drainage layer on the structural performance of a lining is more pronounced for shallow tunnels than for tunnels of greater depth for a given hydraulic head H_w. Such a trend can be attributed to the fact that the confinement stress level around the tunnel lining, which tends to restrain the tunnel lining deformation, is higher for a deep tunnel than for a shallow tunnel. Greater effects of hydraulic deterioration of the drainage layer on the structural performance of a tunnel lining should be anticipated for tunnels constructed at shallower depths than deeper depths for a given H_w.

5.4. Effect of ground type

Figure 20 shows the effect of ground type on the hydraulic deterioration-induced lining force and stress distributions for cases of $H_c = 5D$, $H_w = 5D$. As one can expect, the hydraulic deterioration-induced lining forces, i.e. ΔSF and ΔSM, tend to increase as the ground becomes weaker. These results are rearranged in Figure 21 so that ΔSF and ΔSM at various locations can be related to the uniaxial compressive strength (USC) of the ground, defined as $\sigma_c = 2\ c\ \cos\phi/(1 - \sin\phi)$. As can be observed, the weakest ground GT-I ($\sigma_c = 17$ MPa) yielded ΔSF and ΔSM at the spring line of 0.14 MN and 120 kN-m, respectively, leading to a $\Delta\sigma$ value of 8 MPa. In GT-III ($\sigma_c = 1920$ MPa), more competent ground, ΔSF and ΔSM, thus $\Delta\sigma$ are negligibly small, suggesting no or a negligible

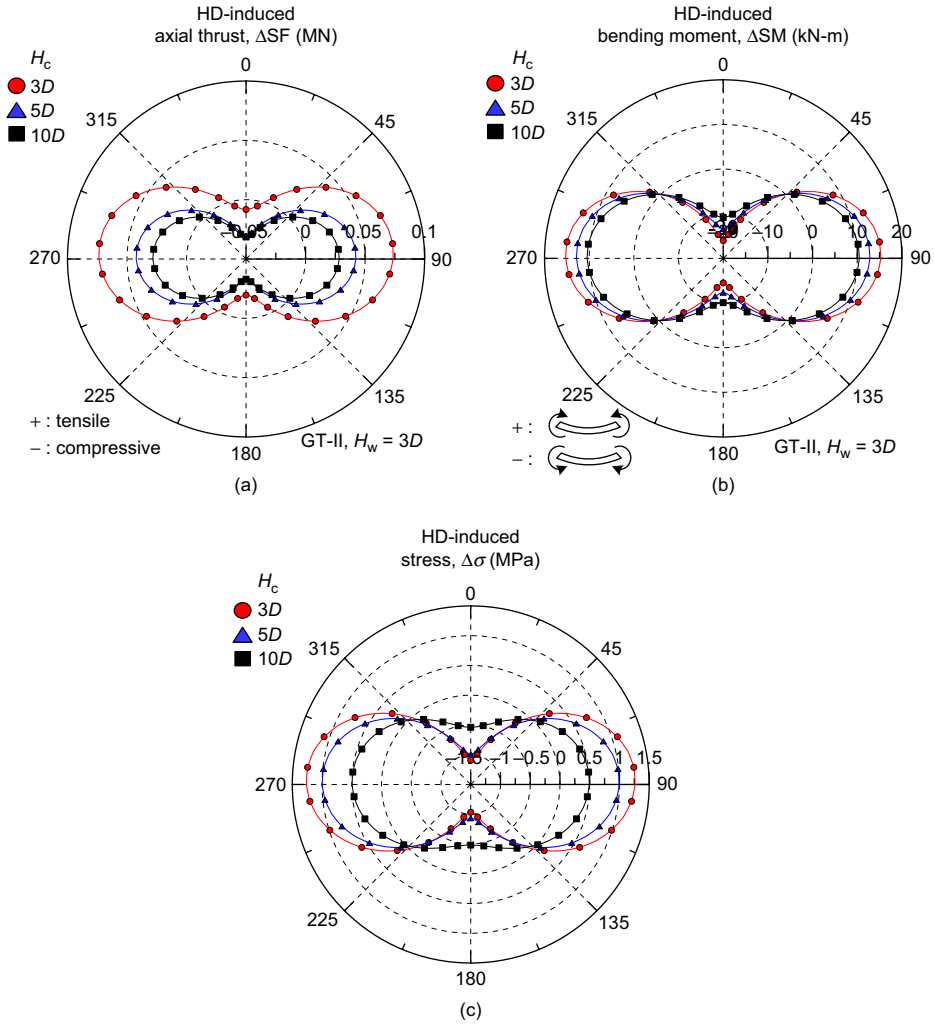

Figure 17. Hydraulic deterioration-induced lining force and stress distributions for various H_c (GT-II, $H_w = 3D$, RP = 1000): (a) ΔSF; (b) ΔSM; (c) $\Delta\sigma$. HD, hydraulic deterioration

effect of decrease in drainage capacity by hydraulic deterioration on the structural performance of the lining.

In terms of percentage increase values from the respective no-hydraulic deterioration cases shown in Figure 22, it can be seen that the bending moment $\Delta SM/SM_{nc}$ shows considerably more pronounced variation with the ground type than the axial thrust $\Delta SF/SF_{nc}$, showing a range of $\Delta SM/SM_{nc}$ from 440% for GT-I to almost zero for GT-III. The resulting percentage increases of stress show $\Delta\sigma/\sigma_{nc}$ as high as 100% for GT-I. These results also confirm that the decrease in drainage capacity of the drainage layer has more significant impact on tunnels constructed in weak ground.

The hydraulic deterioration-induced lining forces and stresses at the spring line are plotted against the hydraulic head H_w in Figure 23. As shown, the rates of increase in $\Delta SF/SF_{nc}$ and $\Delta SM/SM_{nc}$, thus $\Delta\sigma/\sigma_{nc}$, seem to become greater as the ground gets weaker, showing an exponentially increasing pattern for GT-I. These results again demonstrate that the decrease in drainage capacity of the drainage layer can be detrimental to the structural integrity of the lining for tunnels constructed in rather weak ground under high hydraulic head.

6. CONCLUSIONS

In this study, the results of a numerical investigation into the effect of hydraulic deterioration on lining performance are presented specifically for tunnels with drained waterproofing systems. A series of hypothetical tunnel construction scenarios were first developed with due consideration of tunnel cover depth as well as depth of groundwater table, and ground type. In order to realistically model the hydro-mechanical interaction between the ground and the lining that arises due to the deterioration of the drainage system by clogging as well as squeezing, a fully coupled two dimensional stress–pore-pressure FE model was adopted. The results of the analyses are presented so that the structural performance of the lining and the hydro-mechanical ground-lining interaction can be related. The following conclusions can be drawn from the tunnels considered in this study.

(1) Review of a case study, specifically directed to the tunnel drainage filter application of geotextile, revealed that the current geotextile filter design criteria, the clogging resistance criterion in particular, includes some degree of inherited conservatism when

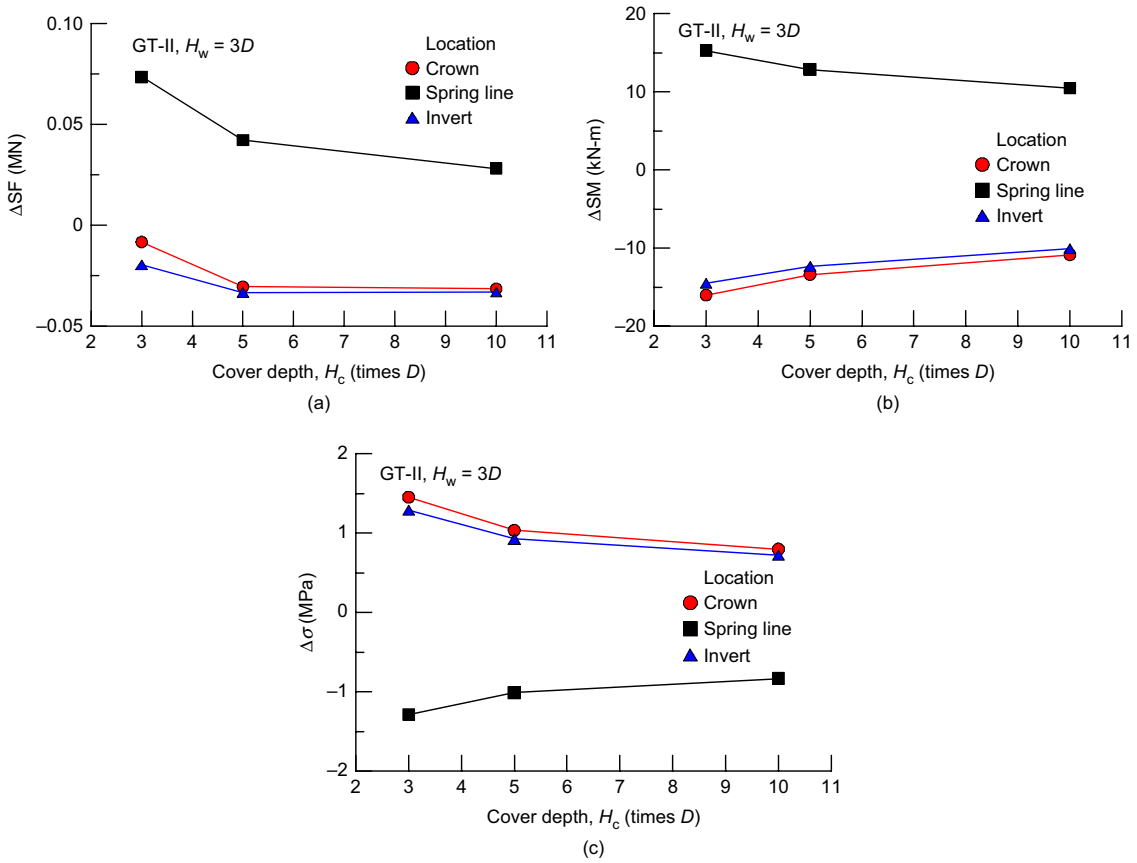

Figure 18. Variation of hydraulic deterioration-induced lining forces and stresses with H_c at various locations (GT-II, $H_w = 3D$, RP = 1000): (a) ΔSF; (b) ΔSM; (c) Δσ

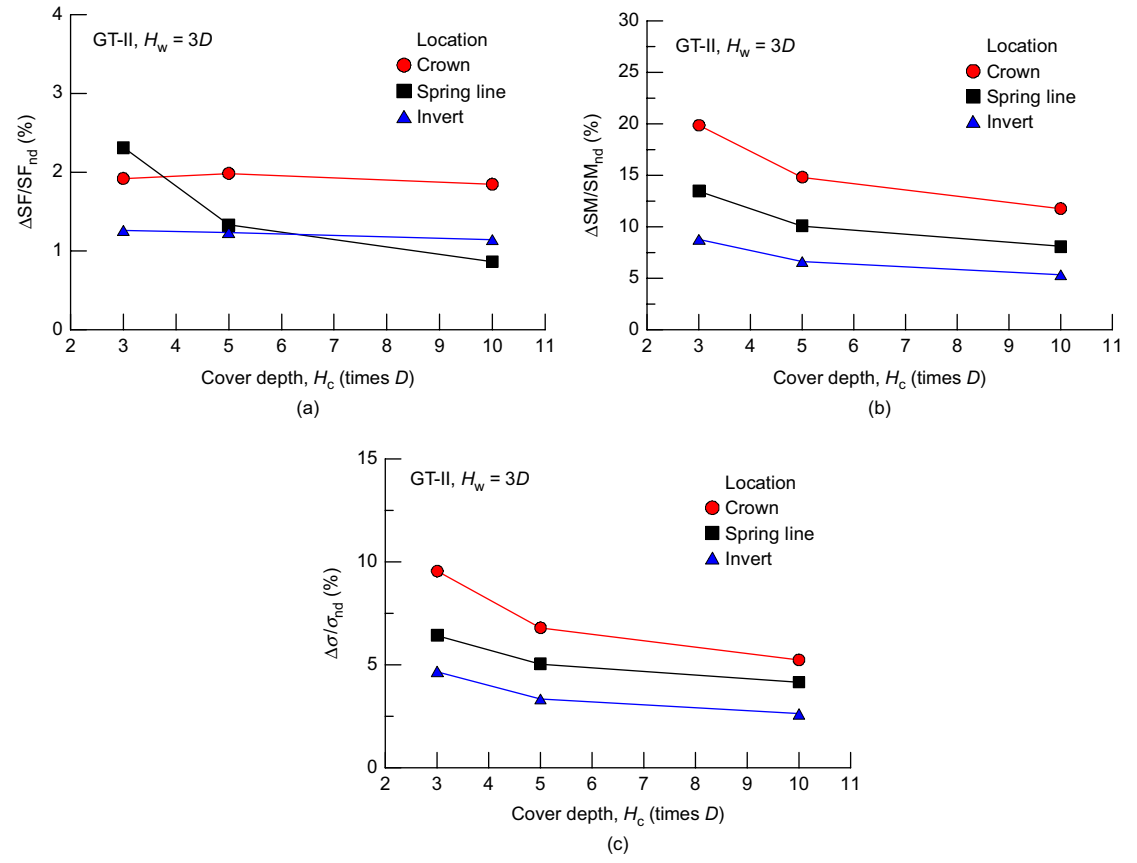

Figure 19. Variation of percent increase in hydraulic deterioration-induced lining forces and stresses with H_c at various locations (GT-II, $H_w = 3D$, RP = 1000): (a) ΔSF/SF$_{nd}$; (b) ΔSM/SM$_{nd}$; (c) Δσ/σ$_{nd}$

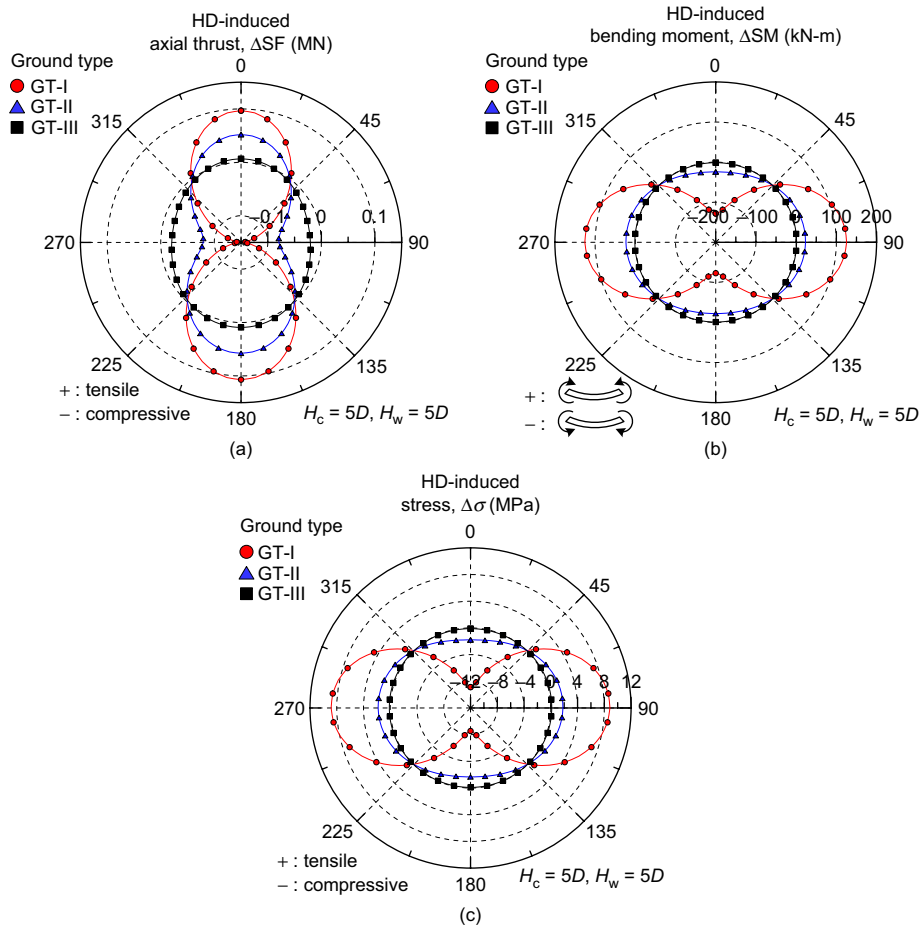

Figure 20. Hydraulic deterioration-induced lining force and stress distributions for various ground types (GT-II, $H_c = 5D$, $H_w = 5D$, RP = 1000): (a) ΔSF; (b) ΔSM; (c) Δσ. HD, hydraulic deterioration

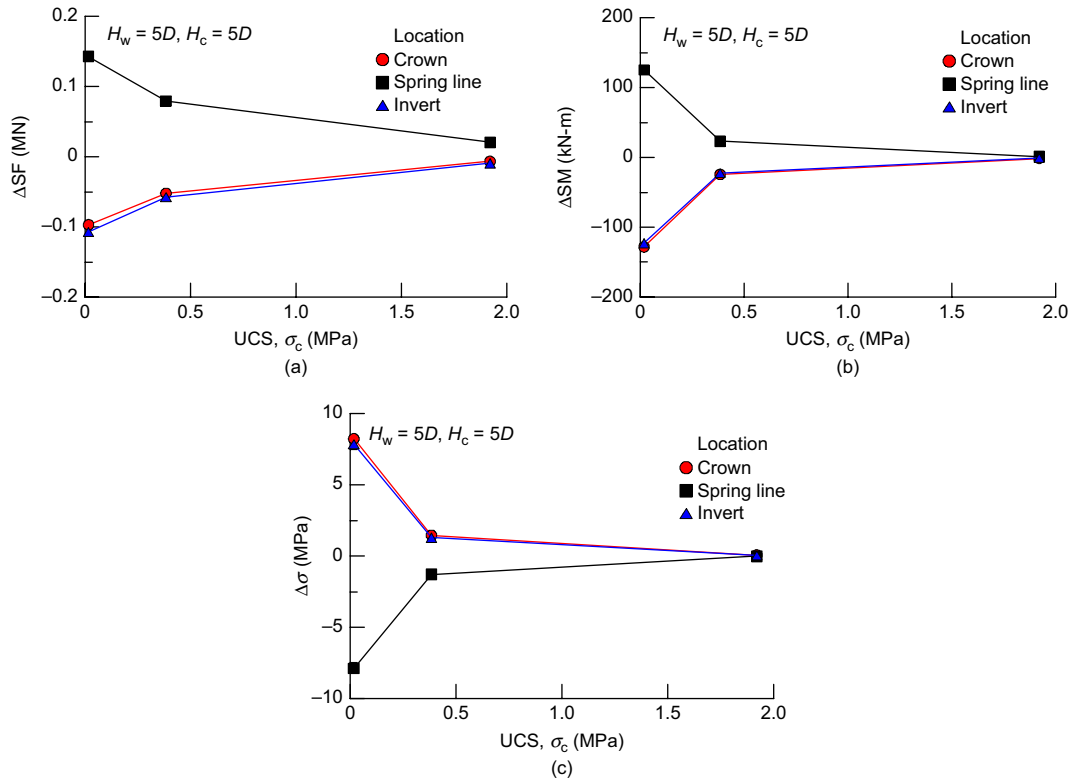

Figure 21. Variation of hydraulic deterioration-induced lining forces and stresses with ground types at various locations (GT-II, $H_c = 5D$, $H_w = 5D$, RP = 1000): (a) ΔSF; (b) ΔSM; (c) Δσ

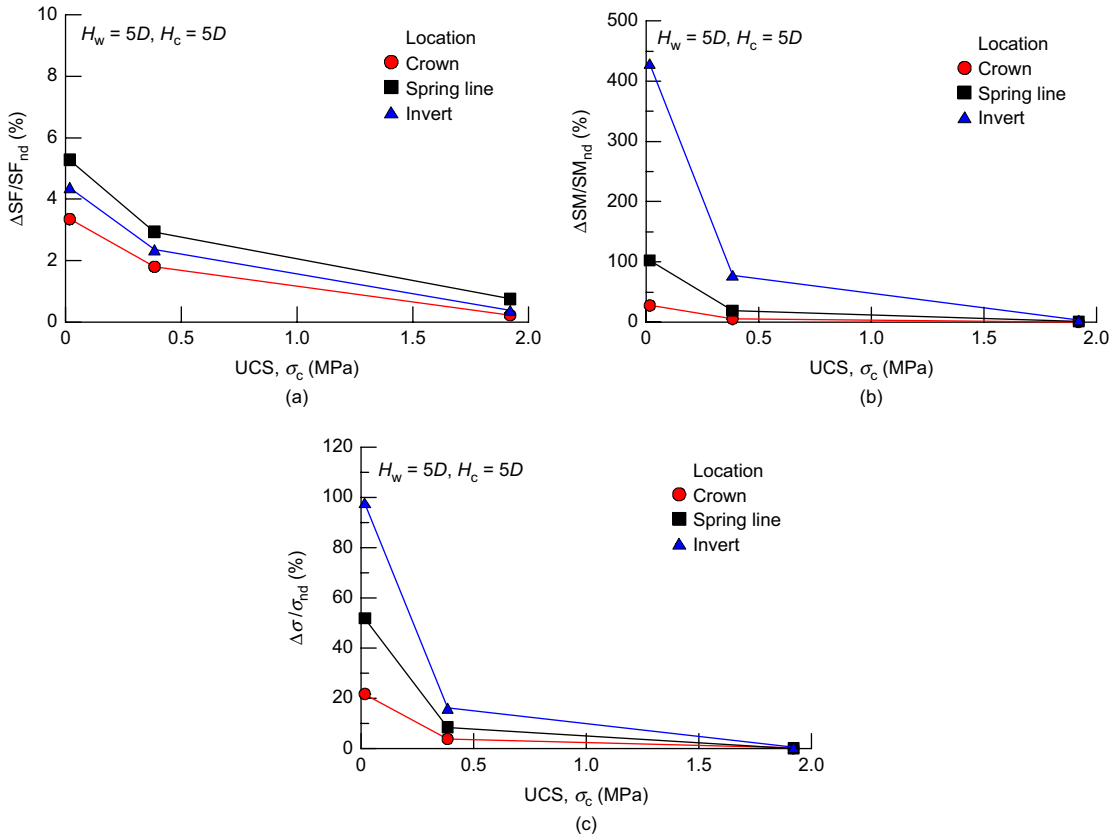

Figure 22. Variation of percent increase in lining forces and stresses with σ_c at various locations (GT-II, $H_c = 5D$, $H_w = 5D$, RP = 1000): (a) ΔSF/SF$_{nd}$; (b) ΔSM/SM$_{nd}$; (c) Δσ/σ$_{nd}$

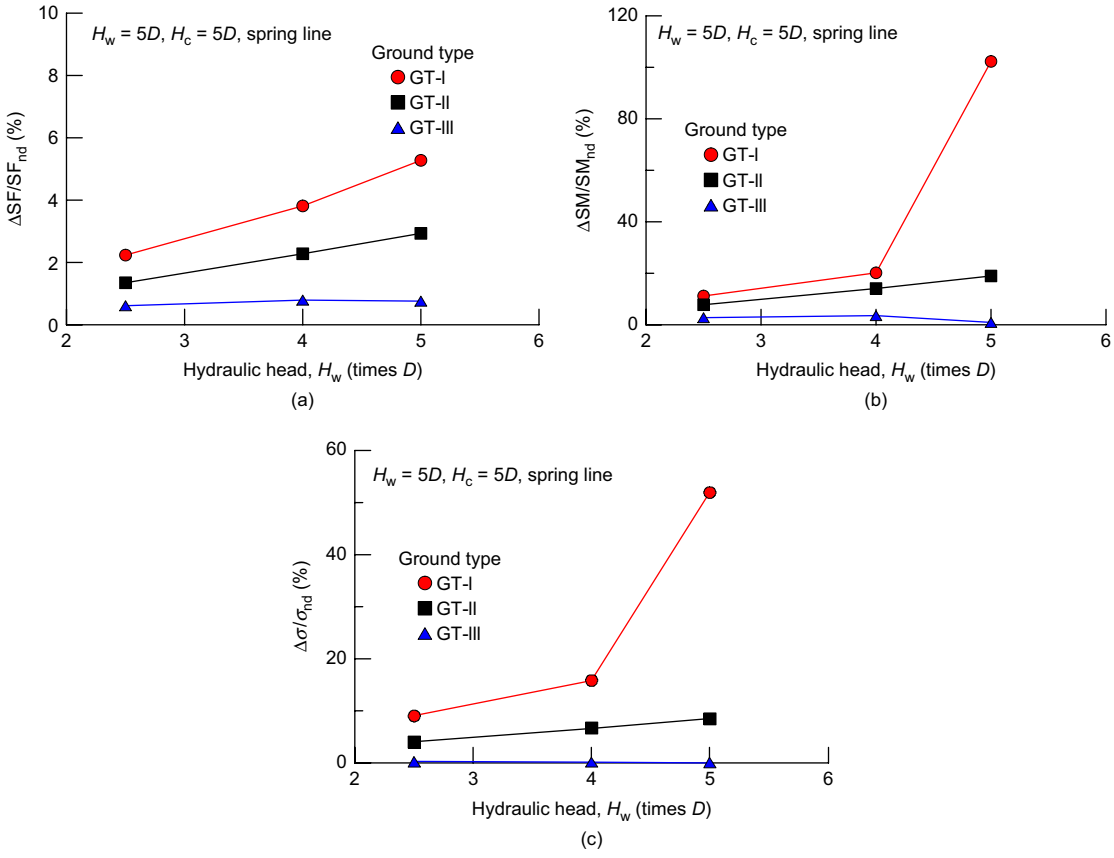

Figure 23. Variation of percent increase in lining forces and stresses at spring line with H_w for various ground types (GT-II, $H_c = 5D$, $H_w = 5D$, RP = 1000): (a) ΔSF/SF$_{nd}$; (b) ΔSM/SM$_{nd}$; (c) Δσ/σ$_{nd}$

compared to the results from the GR test. It is therefore recommended that the GR test be adopted in routine geotextile filter drainage design for tunnels.

(2) The decrease in drainage capacity of a drainage layer by hydraulic deterioration imposes additional lining forces, due to the pore pressure build-up behind the lining, the magnitudes of which are dependent on the degree of hydraulic deterioration of the drainage layer. The hydraulic deterioration-induced lining forces result in increases in the lining stress in tension at the crown and invert levels, but in compression at the spring line.

(3) The hydraulic deterioration-induced lining forces tend to increase with an increase in H_w with the largest increase at the spring line. The percentage increase values of ΔSF and ΔSM from otherwise fully drained case indicate that the percentage increases of axial thrust are much smaller than those of bending moment, suggesting that the pore pressure build-up behind the lining is mainly relevant to the increases in bending moment.

(4) The normalised progressive development of the hydraulic deterioration-induced lining forces can be best fit using a two-term exponential function which can be used to infer hydraulic deterioration-induced lining forces during operation for the range of cases considered in this study, given their respective maximum values.

(5) The hydraulic deterioration-induced lining forces as well as stresses tend to slightly decrease with an increase in the cover depth H_c, suggesting that the effect of decrease in drainage capacity of drainage layer by hydraulic deterioration on the structural performance of a lining may be more pronounced for shallow tunnels than for deep tunnels for a given hydraulic head H_w.

(6) The hydraulic deterioration-induced lining forces, i.e. ΔSF and ΔSM, tend to increase as the ground becomes weaker, implying that the structural integrity of the lining may be significantly affected in the event of hydraulic deterioration of the drainage layer for tunnels constructed in rather weak ground under high hydraulic head.

ACKNOWLEDGEMENTS

This research is supported by Grant No. 13CCTI-T01 from the Ministry of Land, Transport and Maritime Affairs, Korea. Their financial support is gratefully acknowledged. Special thanks go to E-M. Jung, who conducted a series of the numerical analyses in the paper.

NOTATION

Basic SI units are given in parentheses.

C_c coefficient of gradation (dimensionless)
C_u uniformity coefficient (dimensionless)
c' cohesion (kN/m^2)
D tunnel diameter (m)
D_{15} diameter corresponding to 15% finer (mm)
D_{50} diameter corresponding to 50% finer (mm)
D_{85} diameter corresponding to 85% finer (mm)
D_{90} diameter corresponding to 90% finer (mm)
E Young's modulus (MN/m^2)
H_c tunnel cover depth (m)
H_w hydraulic head (m)
K_o lateral stress coefficient (dimensionless)
k_c permeability of concrete (m/s)
k_d permeability of drainage layer (m/s)
k_g permeability of ground (m/s)
O_{95} apparent opening size (mm)
RP relative permeability of drainage to ground (k_g/k_d) (dimensionless)
SF_{nc} final axial thrust with no-deterioration (MN)
SM_{nc} final bending moment with no-deterioration (kN-m)
w_{opt} optimum water content (dimensionless)
ΔSF deterioration-induced axial thrust of lining (MN)
ΔSM deterioration-induced bending moment of lining (kN-m)
$\Delta\sigma$ deterioration-induced lining stress of lining (MPa)
ϕ' internal friction angle (°)
γ_d dry unit weight (kN/m^3)
γ_{sat} saturated unit weight (kN/m^3)
σ_{nc} final lining stress with no-deterioration (MPa)
υ Poisson's ratio (dimensionless)

REFERENCES

Abaqus (2011). *Abaqus Users Manual, Version 6.13*, Hibbitt, Karlsson, and Sorensen, Inc., Pawtucket, Providence, RI, USA.

ASTM D5101-12 *Standard Test Method for Measuring the Filtration Compatibility of Soil–Geotextile Systems.* ASTM International, West Conshohoken, PA, USA.

Bilfinger, W. (2005). Impermeabilization versus drainage – some considerations regarding lining loads. *Felsbau Rock and Soil Engineering*, **23**, No. 3, 55–61.

Celestino, T. B. (2005). Shotcrete and waterproofing for operational tunnels. *ITA Working Group 12 on Sprayed Concrete Use*, Working Group Report, International Tunnelling and Underground Space Association, Lausanne, CH.

CFCC (French Committee on Geotextiles and Geomembranes) (1986). *AFNOR G38017*, Association Francaise de Normalisation, Boulogne-Billancourt, France (in French).

Christopher, B. R. & Fischer, G. R. (1992). Geotextile filtration principles, practices and problems. *Geotextiles and Geomembranes*, **11**, No. 4–6, 337–353.

Christopher, B. R. & Holtz, R. D. (1985). *Geotextile Engineering Manual. U.S. Federal Highway Administration*, Report FHWA-TS-86/203. National Highway Institute, Washington, DC, UK.

Davis, E. H. (1968). Theories of plasticity and the failure of soil masses. *Soil Mechanics: Selected Topics*, Lee, I. K., Editor, Butterworth's, London, UK, pp. 341–380.

Fischer, G. R., Christopher, B. R. & Holtz, R. D. (1990). Filter criteria based on pore size distribution. *Fourth International Conference on Geotextiles, Geomembranes and Related Products*, Den Hoedt, G., Editor. Balkema, The Hague, The Netherland, pp. 289–294.

Franzen, T. & Celestino, T. B. (2002). Lining of tunnels underground water pressure. *AITES-ITA World Tunnel Congress*, Sydney, pp. 481–487.

Huang, C. J., Monsees, J., Munfah, N. & Wisniewski, J. (2009). *Technical Manual for Design and Construction of Road Tunnels – Civil Elements. U.S. Federal Highway Administration*, Final Report

FHWA/NHI-10-034. National Highway Institute, Washington, DC, USA.

Jung, H. S., Han, Y. S., Chung, S. R., Chun, B. S. & Lee, Y. J. (2013). Evaluation of advanced drainage treatment for old tunnel drainage system in Korea. *Tunnelling and Underground Space Technology*, **38**, No. 6, 475–486.

Koerner, R. M. (1990). *Designing with Geosynthetics*, 2nd edn, Prentice Hall, Englewood Cliffs, NJ, USA.

Koerner, R. M. (2012). *Designing with Geosynthetics*, 6th edn, vol. 1, Xlibris Corporation, Lexington, KY, USA.

Kolymbas, D. (2005). *Tunnelling and Tunnel Mechanics – A Rational Approach to Tunnelling*, 1st edn, Springer, Berlin, Germany.

Lafleur, J. (1999). Selection of geotextiles to filter broadly graded cohesionless soils. *Geotextiles and Geomembranes*, **17**, No. 5–6, 299–312.

Lee, I. M., Yu, S. H., Park, K. J., Lee, S. W. & Kim, H. T. (1999). Clogging phenomenon and drainage capacity of tunnel filters. *Journal of Korean Geotechnical Society*, **15**, No. 5, 3–18.

Lee, S. & Bourdeau, P. L. (2006). *Filter Performance and Design for Highway Drains. U.S. Federal Highway Administration*, Final Report FHWA/IN/JTRP-2005/1. National Highway Institute, Washington, DC, USA.

Moon, J. S. (2000). *A Study on Clogging and Hydraulic Properties for Drain Filters of Tunnels*, MSc thesis, Dongkuk University, Seoul, Korea.

Murillo, C. A., Shin, J. H., Kim, K. H. & Colmenares, J. E. (2014). Performance tests of geotextile permeability for tunnel drainage system. *KSCE J. Civil Engineering*, **18**, No. 3, 827–830.

Palmeira, E. M. & Fannin, R. J. (2002). Soil-geotextile compatibility in filtration. *Seventh International Conference on Geosynthetics*, Delmas, Ph. and Gourc, J. P., Editors. Balkema, Nice, France, pp. 853–870.

Park, K. J. (1999). *Analysis of Particle Mobilization and Impact on Filter Performance in Drainage Tunnels*, PhD thesis, Korea University, Seoul, Korea.

Rollin, A. L. & Lombard, G. (1988). Mechanisms affecting long-term filtration behavior of geotextile. *Geotextiles and Geomembranes*, **7**, No. 1–2, 119–145.

Shin, J. H. (2008). Numerical modeling of coupled structural hydraulic interactions in tunnel linings. *Structural Engineering and Mechanics*, **29**, No. 1, 1–16.

Shin, J. H. & Potts, D. M. (2002). Time-based two dimensional modelling of NATM tunnelling. *Canadian Geotechnical Journal*, **39**, No. 3, 710–724.

Shin, J. H., Potts, D. M. & Zdravkovic, L. (2005). The effect of pore-water pressure on NATM tunnel linings in decomposed granite soil. *Canadian Geotechnical Journal*, **42**, No. 6, 1585–1599.

Shin, J. H., Lee, I. K. & Joo, E. J. (2014). Behavior of double lining due to long-term hydraulic deterioration of drainage system. *Structural Engineering and Mechanics*, **52**, No. 6, 1257–1271.

Waltham, A. C. (1994). *Foundations of Engineering Geology*, Blackie Academic & Professional, London, UK.

Yoo, C. (2005). Interaction between tunnelling and groundwater – numerical investigation using three dimensional stress-pore pressure coupled analysis. *Journal of Geotechnical and Geoenvironmental Engineering*, **131**, No. 2, 240–250.

Yoo, C. & Kim, S. B. (2008). Three-dimensional numerical investigation of multifaced tunnelling in water-bearing soft ground. *Canadian Geotechnical Journal*, **45**, No. 10, 1467–1486.

Yoo, C., Lee, Y., Kim, S. H. & Kim, H. T. (2012). Tunnelling-induced ground settlements in a groundwater drawdown environment – a case history. *Tunnelling and Underground Space Technology*, **29**, No. 3, 69–77.

The Editor welcomes discussion on all papers published in Geosynthetics International. Please email your contribution to discussion@geosynthetics-international.com.